Steel and Composite Structures, *Vol. 23, No. 5 (2017) 517-527*
DOI: https://doi.org/10.12989/scs.2017.23.5.517

Experimental study and calculation of laterally-prestressed confined concrete columns

Mahdi Nematzadeh [*1], Saeed Fazli [1a] and Iman Hajirasouliha [2b]

[1] *Department of Civil Engineering, University of Mazandaran, Babolsar, 47416-13534, Iran*
[2] *Department of Civil and Structural Engineering, University of Sheffield, Sheffield, UK*

(*Received November 04, 2016, Revised January 20, 2017, Accepted January 24, 2017*)

Abstract. In this paper, the effect of active confinement on the compressive behaviour of circular steel tube-confined concrete (STCC) and concrete-filled steel tube (CFST) columns is investigated. In STCC columns the axial load is only applied to the concrete core, while in CFST columns the load is carried by the whole composite section. A new method is introduced to apply confining pressure on fresh concrete by laterally prestressing steel tubes. In order to achieve different prestressing levels, short-term and long-term pressures are applied to the fresh concrete. Three groups of STCC and CFST specimens (passive, S-active and L-active groups) are tested under axial loads. The results including stress-strain relationships of composite column components, secant modulus of elasticity, and volumetric strain are presented and discussed. Based on the elastic–plastic theory, the behaviour of the steel tube is also analyzed during elastic, yielding, and strain hardening stages. The results show that using the proposed prestressing method can considerably improve the compressive behaviour of both STCC and CFST specimens, while increasing the prestressing level has insignificant effects. By applying prestressing, the linear range in the stress–strain curve of STCC specimens increases by almost twice as much, while the improvement is negligible in CFST specimens.

Keywords: prestressing; stress–strain; elastic-plastic theory; confined concrete; steel tube; active confinement

1. Introduction

Steel tube-confined concrete (STCC) and concrete-filled steel tube (CFST) members are widely used in many modern structures due to their high strength, stiffness, and ductility. In STCC columns, the loading is applied only to the concrete core, while in CFST columns, the composite section is loaded. STCC and CFST columns exhibit better performance compared to conventional concrete and steel columns as a result of the composite action of the concrete core and steel tube. However, the two types of composite columns demonstrate different compressive behavior, which is caused by different behaviors of their steel tube component. The steel tube in STCC columns plays a more confining and less axial load-carrying role in comparison with that of CFST columns, leading to significantly reduced possibility of steel tube local buckling in STCC relative to CFST columns (Aboutaha and Machado 1998). In addition, considering the ductility and strength of the composite columns as the most important design factors, application of the STCC section is recommended (Yu *et al*. 2010). On the other hand, in case that the column stiffness is regarded as the most important design factor, or that the longitudinal reinforcing role of the steel tube is of greater importance without the need for additional reinforcement, the CFST section can be employed (Tokgoz and Dundar 2010).

Valuable studies on the performance of STCC (Aboutaha and Machado 1998, Han *et al*. 2005, Fu *et al*. 2011, Huang *et al*. 2012) and CFST columns (Wan and Zha 2016, Hua *et al*. 2014, Kim *et al*. 2013) under axial compression are found in the literature. Huang *et al*. (2012) investigated the mechanical behavior of circular steel tube-confined recycled aggregate concrete, and found that the longitudinal stress of the steel tube is reduced after yielding. In addition, the secant modulus of hoop stress reaches its maximum value at the steel yielding point and decreases afterwards. Lai and Ho (2014) studied CFST columns confined by tie bars and rings under uniaxial load. They showed that the steel tube axial vs. lateral strain increases linearly. The compressive behavior of CFST columns was investigated experimentally and numerically by Abed *et al*. (2013). They concluded that by reducing the diameter to thickness ratio of the steel tube, the ultimate strength, ductility, and toughness of CFST columns increases, and for a given ratio, with increasing concrete compressive strength, the load-carrying capacity of the composite section also increases.

Although significant studies have been carried out on the STCC and CFST columns individually, little research has been devoted to comparing their performance with each other in the literature. Yu *et al*. (2010) investigated the compressive behavior of STCC columns and compared it with CFST columns. They found that the axial force of the steel tube in STCC columns is lower compared to that of CFST columns while the confining pressure applied to the

*Corresponding author, Assistant Professor,
E-mail: m.nematzadeh@umz.ac.ir
[a] Graduate Student, E-mail: Saeed_fazli_1368@yahoo.com
[b] Assistant Professor,
E-mail: i.hajirasouliha@sheffield.ac.uk

ISSN: 1229-9367 (Print), 1598-6233 (Online)

concrete core in STCC columns is higher.

The confinement in STCC and CFST columns is accomplished by two approaches: passive and active. In the passive confinement, before the compressive load is applied, no lateral pressure acts on the concrete core; hence, a large lateral deformation is required to create an effective confinement. One way to avoid this and the resulting cracks is to use an active confinement, in which a lateral confining pressure is applied to the concrete core before the loading, resulting in a delayed crack formation and an improved compressive behavior of composite columns.

To date, the methods for prestressing the composite columns and creating the active confinement have been limited, with some of them acting by pre-tensioning and the others by post-tensioning. Use of the expansive material in the concrete mixture (Mortazavi *et al*. 2003, Chang *et al*. 2009) and prestressing the transverse hoops (Shinohara 2008) are the most commonly used methods for lateral pre-tensioning. Moreover, prestressing the continuous spiral band (Janke *et al*. 2009) or individual strips (Moghaddam *et al*. 2010), thermal prestressing of the steel-confining components (Mokari and Moghadam 2008), and use of the self-stressing composites (Krstulovic-Opara and Thiedeman 2000, Shin and Andrawes 2010) are the most notable procedures for lateral post-tensioning. In all these studies, an improvement in the mechanical performance of the composite column having active confinement relative to passive one was reported.

Based on the literature review, it may be concluded that there is still a lack of knowledge regarding the behavior of the composite sections with active confinement. Therefore, this research aimed to evaluate the effect of prestressing or active confinement on the mechanical behavior of circular STCC and CFST columns under axial compression. In this study, a new technique was employed to prestress the confined stub columns, in which by applying pressure on the fresh concrete poured inside the steel tube, the concrete core was compressed and simultaneously, the steel tube was pre-tensioned in the circumferential direction. In order to assess the effect of the prestressing level on the behavior of STCC and CFST columns, the pressure was applied to the fresh concrete in two ways, i.e., short-term and long-term. Here, the steel tube was analyzed in the elastic, yielding, and strain hardening stages based on the elastic-plastic theory along with the proposed simple method. The results suggested that prestressing considerably improved the compressive behavior of the STCC and CFST columns, while increasing the pre-stressing level had a negligible effect.

2. Experimental program

2.1 Specimens and materials

In total, 18 composite specimens divided into the two groups of STCC and CFST were tested in this study. Each group consisted of the passive specimens, short-term prestressed steel tube-confined compressed concrete (S-active) specimens, and long-term prestressed steel tube-confined compressed concrete (L-active) specimens. Three identical specimens were prepared for each test, with the reported value being the mean of the three test results. The concrete core length in the STCC and CFST specimens with passive confinement was 140 mm while in specimens with active confinement, this length was 17 mm shorter. On the other hand, the initial length of the steel tube in all the specimens was 150 mm.

In the STCC specimens, the distance between the ends of the concrete core and steel tube was filled with a solid steel cylinder in order to transfer the compressive load only to the concrete core. In the CFST specimens, since the load must be applied to the steel-concrete composite section, the two ends of the steel tube were cut to the extent that the end surfaces of the concrete and steel were at the same level.

The steel tube used in this study was of the seamless type. The mechanical and geometrical properties of the steel tube are presented in Table 1. Here, D and t are the outer diameter and wall thickness of steel tube; ε_p and ε_u are strains at the strain hardening and ultimate points; f_y and f_{us} are yield strength and ultimate strength; v_s is Poisson's ratio; and E_s and E'_s are the initial modulus of elasticity and strain hardening modulus of elasticity, respectively.

Concrete mix design is in accordance with the ACI 211 (2000) requirements. In all of the concrete mixes, the crushed coarse aggregate with the maximum size of 12.5 mm, fluvial sand, and Type I Portland cement were used with no additives. The compressive strength of the reference concrete and short- and long-term compressed unconfined concrete were 33.5, 66.2, and 69.4 MPa, respectively.

2.2 Test setup and instrumentation

Compression tests on the STCC and CFST specimens were carried out after at least 28 days had passed from the concreting date by using a 2000 kN capacity ELE testing machine. The composite specimens were loaded at the slow rates of 0.7 kN/s or 0.29 MPa/s, which was the same as the unconfined concrete loading rate and well within the range

Table 1 Experimental properties of steel tube

t (mm)	D (mm)	E_s (GPa)	E'_s (GPa)	v_s	f_y (MPa)	f_u (MPa)	ε_p (ε)	ε_u (ε)
2.5	60.5	210	1.4	0.28	339	480	0.0139	0.1144

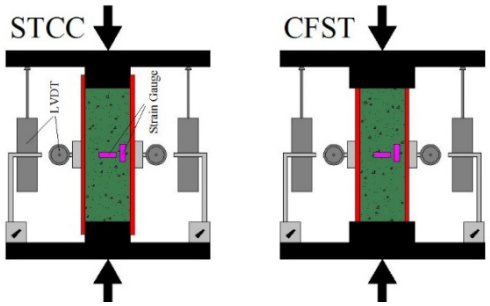

Fig. 1 Schematic view of the load application on CFST and STCC specimens along with the deformation measurement devices

of 0.15-0.35 MPa/s as recommended by the ASTM C39 (2002). The compression test was terminated when the specimens failed.

Axial deformation of the composite specimens was measured by two vertical LVDTs mounted symmetrically on both sides of the specimens between the upper and lower platens of the testing machine. The longitudinal and hoop strains of the steel tubes were measured by the strain gauges installed on the outer surface of the steel tubes at the mid-height. Moreover, to measure large deformations of the specimens in the lateral direction, two horizontal LVDTs were utilized. Fig. 1 shows a schematic view of the loading conditions of the STCC and CFST specimens along with the location of the deformation measurement instruments.

2.3 Prestressing apparatus

To create active confinement, the STCC and CFST specimens were placed inside the prestressing apparatus (see Fig. 2). This apparatus is able to apply a specified amount of pressure to the specimens for any given duration. Circular steel tubes filled with fresh concrete were put in the pressure apparatus in a successive manner and separated from each other by solid steel covers, as shown in Fig. 2. The axial pressure was applied to the fresh concrete in the first concrete specimen by using a hydraulic jack installed on top of the apparatus. Then, the pressure was transferred to the next specimens through steel covers centrally located between the successive specimens. The further details of the pressure apparatus are provided in the previous papers (Nematzadeh and Naghipour 2012, Nematzadeh *et al*. 2017). By using this technique, the steel tubes became pre-tentioned and the fresh concrete became compressed accordingly. The pressure was applied to the specimens in two ways, i.e., short-term and long-term, to obtain low and high prestressing levels, respectively. The short-term pressure in the S-active and the long-term pressure in the L-active specimens lasted for 15-30 minutes and 6 days, respectively.

Values of the initial and final pressure (prestressing level), and the pressure loss in the CFST and STCC specimens were calculated using the circumferential strain of the steel tubes measured by the strain gauges mounted on the outer wall of the steel tube. The initial hoop strain of the S-active and L-active specimens after applying a constant pressure was equal to 762.8 microstrain. After removing the S-active specimens from the prestressing apparatus, a considerable sudden drop was observed in the initial strain of the steel tube; however, its value did not reach zero. This observation can be attributed to the internal friction between the aggregate grains (Nematzadeh and Naghipour 2012). In addition, the shrinkage is one of the important factors contributing to daily pressure loss, which decreases over time. By taking the L-active specimens out of the prestressing apparatus, a smaller pressure loss occurred compared to that of the S-active specimens. The final strain of the S-active and L-active specimens after a 28-day pressure application period was 94.0 and 374.3 microstrain, respectively, equivalent to the confining pressures of 1.78 and 7.08 MPa, respectively.

Fig. 2 Prestressing apparatus

3. Analysis of steel tube

The longitudinal and hoop stresses of the steel tube during axial loading were calculated by applying the elastic–plastic analysis method to the measured strains of the steel tube. In this study, for the STCC and CFST specimens, a trilinear stress–strain curve of steel tube was employed, which consists of the three stages called elastic, yield, and strain hardening. Therefore, the analytical calculations must be performed in three stages. It should be noted that the shear stress at the steel tube mid-height where the strain gauges were installed was zero, hence, the corresponding normal stresses were considered as the principal stresses. Furthermore, the radial stress on the outer surface of the steel tube where the strain gauges were mounted was zero. In this study, the yield criterion used for steel was the von Mises yield criterion (Hosford 2010).

3.1 Analysis in elastic stage

The longitudinal and hoop stresses of a steel tube in the elastic stage can be obtained through the classic material strength relationships expressed as Eqs. (1) and (2), respectively.

$$\sigma_v = \left(\frac{E_s}{1-v_s^2}\right)\left[\varepsilon_v + v_s\varepsilon_h\right] \tag{1}$$

$$\sigma_h = \left(\frac{E_s}{1-v_s^2}\right)\left[\varepsilon_h + v_s\varepsilon_v\right] \tag{2}$$

where ε_v and ε_h are the longitudinal and hoop strains of the steel tube; σ_v and σ_h are the longitudinal and hoop stresses of the steel tube, respectively. Additionally, E_s and v_s are the modulus of elasticity and Poisson's ratio of the steel tube given in Table 1.

In the elastic stage, the total equivalent stress defined as Eq. (3) is lower than the yield stress of steel tube ($\sigma_{eq} < f_y$).

$$\sigma_{eq} = \sqrt{\sigma_h^2 + \sigma_v^2 - \sigma_h\sigma_v} \tag{3}$$

In the above equation, σ_{eq} is the total equivalent stress of the steel tube.

3.2 Analysis in yield stage

Once the total equivalent stress of a steel tube passes the yield stress ($\sigma_{eq} = f_y$), the steel enters the yielding stage; the end of which denotes the starting point of the steel tube strain hardening stage. The general equation governing the strains and stresses in the yielding stage is referred to as the flow rule written as follows

$$d\varepsilon_{ij}^{p} = d\lambda\left(\frac{\partial f}{\partial \sigma_{ij}}\right) \tag{4}$$

where σ_{ij} is the principal stress, and ε_{ij}^{p} is the principal plastic strain. Moreover, $d\lambda$ is a constant value depending on the shape of stress–strain curve, and f is the yield function corresponding to the yield criterion. Based on the von Mises yield criterion, f can be written as a function of the principal stresses as follows

$$f = \frac{1}{4}[(\sigma_r - \sigma_h)^2 + (\sigma_r - \sigma_v)^2 + (\sigma_h - \sigma_v)^2] \tag{5}$$

By substituting Eq. (5) into Eq. (4), the following equations are obtained

$$\begin{cases} d\varepsilon_r^p = d\lambda\left[\sigma_r - \dfrac{(\sigma_h + \sigma_v)}{2}\right] \\ d\varepsilon_h^p = d\lambda\left[\sigma_h - \dfrac{(\sigma_r + \sigma_v)}{2}\right] \\ d\varepsilon_v^p = d\lambda\left[\sigma_v - \dfrac{(\sigma_r + \sigma_h)}{2}\right] \end{cases} \tag{6}$$

where $d\varepsilon_r^p$, $d\varepsilon_h^p$, and $d\varepsilon_v^p$ are the plastic strain increments in the radial, hoop, and longitudinal directions of the steel tube, respectively. By defining the stress ratio as $\alpha = \dfrac{\sigma_v}{\sigma_h}$ and the ratio of the plastic strain increments as $\beta = \dfrac{d\varepsilon_v^p}{d\varepsilon_h^p}$, a simple method can be used for the steel tube analysis. Considering the absence of radial stress on the tube outer wall ($\sigma_r = 0$), it can be written

$$\beta = \frac{2\alpha - 1}{2 - \alpha} \tag{7}$$

Using the von Mises equation ($\sqrt{\sigma_h^2 + \sigma_v^2 - \sigma_h\sigma_v} = f_y$), the longitudinal and hoop stresses in the yielding stage can be expressed in terms of the parameter α as Eq. (8), and the stress increments can be written as Eq. (9).

$$\begin{cases} \sigma_h = \dfrac{f_y}{\sqrt{\alpha^2 - \alpha + 1}} \\ \sigma_v = \dfrac{\alpha f_y}{\sqrt{\alpha^2 - \alpha + 1}} \end{cases} \tag{8}$$

$$\begin{cases} d\sigma_h = \dfrac{(1 - 2\alpha) f_y}{2\sqrt{(\alpha^2 - \alpha + 1)^3}} d\alpha \\ d\sigma_v = \dfrac{(2 - \alpha) f_y}{2\sqrt{(\alpha^2 - \alpha + 1)^3}} d\alpha \end{cases} \tag{9}$$

Since the plastic strain is defined as the difference between the total strain and the elastic strain corresponding to the stress, the parameter β is given by the following equation

$$\beta = \frac{d\varepsilon_v - d\varepsilon_v^e}{d\varepsilon_h - d\varepsilon_h^e} = \frac{d\varepsilon_v - \left(\dfrac{d\sigma_v}{E} - v_s\dfrac{d\sigma_h}{E}\right)}{d\varepsilon_h - \left(\dfrac{d\sigma_h}{E} - v_s\dfrac{d\sigma_v}{E}\right)} \tag{10}$$

where ε_h^e and ε_v^e are the elastic strains corresponding to σ_h and σ_v, respectively. Based on the equality of Eqs. (7) and (10), the following equation can be derived.

$$\frac{2E_s d\varepsilon_v \sqrt{(\alpha^2 - \alpha + 1)^3} - (2 - \alpha - v_s + 2v_s\alpha) f_y d\alpha}{2E_s d\varepsilon_h \sqrt{(\alpha^2 - \alpha + 1)^3} - (1 - 2\alpha - 2v_s + v_s\alpha) f_y d\alpha} = \frac{2\alpha - 1}{2 - \alpha} \tag{11}$$

Since the strain increments $d\varepsilon_h$ and $d\varepsilon_v$ are extracted from the strain gauges' data and thus are known values, the only unknown value in the equation is α, which can be determined by applying a numerical method to the equation. In each loading step, $d\alpha$ is considered as the difference between α in that step with the stress ratio obtained in the previous one. After determining α, the values of longitudinal and hoop stresses can be calculated by employing Eq. (8).

To facilitate the calculations performed for reaching the solution in the yielding stage, an appropriate approximation method might be used. Hence, an approximation method was utilized here, in which in order to determine the ratio of the plastic strain increments (β), the elastic strains in each loading step (ε_v^e and ε_h^e) were replaced by the elastic strains corresponding to the starting point of yield stage (ε_v^{ei} and ε_h^{ei}), giving the following

$$\beta = \frac{\varepsilon_v - \varepsilon_v^{ei}}{\varepsilon_h - \varepsilon_h^{ei}} \tag{12}$$

By equating Eq. (7) and Eq. (12), the following equation is achieved, where α is the only unknown.

$$\frac{\varepsilon_v - \varepsilon_v^{ei}}{\varepsilon_h - \varepsilon_h^{ei}} = \frac{2\alpha - 1}{2 - \alpha} \tag{13}$$

In each loading step, independent of the previous analysis step, by using Eq. (8), it is possible to obtain α, and then determine the longitudinal and hoop stresses. The steel tube stress values for one of the specimens, which were obtained by the employed approximation method, are presented in Fig. 3. In this figure, the vertical axis

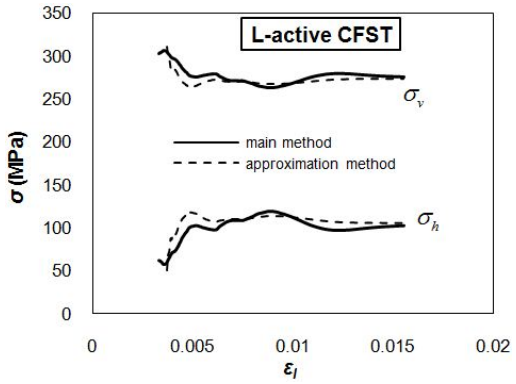

Fig. 3 Comparison of the analytical results of steel tube stresses between the approximation and main method in the yielding stage

represents the longitudinal and hoop stresses of the steel tube in the yielding stage, and the horizontal axis represents the axial strain of the composite column (ε_l). As can be seen, a good agreement exists between the approximation results and those obtained by the main method.

It should be noted that in the equations presented so far, α and β are defined for the analysis of STCC specimens, and hence for CFST specimens, these parameters are expressed as the hoop to longitudinal stress ratio, and the hoop to longitudinal plastic strain increments ratio, respectively. The reason for reversing the parameters α and β for CFST specimens is the fact that the steel tube hoop stress in passive CFST specimens is negligible until the beginning of the yielding stage, hence, Eq. (11) or Eq. (13) cannot be solved.

3.3 Analysis in strain hardening stage

When the total equivalent stress of steel tube becomes greater than its yield stress ($\sigma_{eq} > f_y$), the steel enters the strain hardening stage. Given that the stress–strain curve of steel in this stage is usually assumed to be linear, its slope is considered as the modulus of elasticity of the strain hardening stage (E'_s), which is about 1% of the initial modulus of elasticity. The value of E'_s for the steel tubes used in this study was measured to be 1.4 GPa, as given in Table 1. Based on the anisotropic hardening model, the strain hardening effect can expand the geometric location of the yield surface without changing its shape, and as a result, the yield stresses can increase proportionally in all loading paths. Hence, the axial stress in the strain hardening stage (f_{Hi}) can be calculated from the following

$$f_{Hi} = f_y + E'_s \varepsilon' \tag{14}$$

where ε' is the equivalent strain expressed by Eq. (15). By substituting the generalized Hooke's law into the von Mises equation and assuming $\nu'_s = 0.5$, in which ν'_s is the steel Poisson's ratio in the inelastic stage, the following equation is achieved

$$\varepsilon' = \frac{1}{3}\sqrt{2\left[\left(\varepsilon'_r - \varepsilon'_h\right)^2 + \left(\varepsilon'_h - \varepsilon'_v\right)^2 + \left(\varepsilon'_r - \varepsilon'_v\right)^2\right]} \tag{15}$$

where

$$\begin{cases} \varepsilon'_r = \varepsilon_r - \varepsilon_r^H \\ \varepsilon'_h = \varepsilon_h - \varepsilon_h^H \\ \varepsilon'_v = \varepsilon_v - \varepsilon_v^H \end{cases} \tag{16}$$

in which ε_r^H, ε_h^H, and ε_v^H are the radial, hoop, and longitudinal strains of the steel tube, respectively, at the strain hardening stage starting point; their corresponding values are obtained from the results at the end of yield stage. Since the volumetric plastic strain in the yield and strain hardening stages is zero, the following can be written

$$\varepsilon_r + \varepsilon_h + \varepsilon_v = \varepsilon_r^e + \varepsilon_h^e + \varepsilon_v^e \tag{17}$$

in which the strain ε_r can be expressed as Eq. (18).

$$\varepsilon_r = \frac{\left(1+2\nu_s\right)}{E_s}\left(\sigma_h + \sigma_v\right) - \varepsilon_h - \varepsilon_v \tag{18}$$

Considering that $\alpha = \dfrac{\sigma_v}{\sigma_h}$, Eq. (18) can be rewritten in terms of α as Eq. (19), in which α is the only unknown.

$$\varepsilon_r = \frac{\left(1+2\nu_s\right)}{E_s}\frac{\left(1+\alpha\right)}{\sqrt{\alpha^2 - \alpha + 1}} f_H - \varepsilon_h - \varepsilon_v \tag{19}$$

Now, by replacing f_y in Eqs. (8), (9), and (11), f_H by from the above equation, it is possible to obtain the value of α and subsequently the values of σ_h and σ_v in the steel tube strain hardening stage.

4. Results and discussion

Based on the longitudinal and hoop stresses of the steel tube calculated by applying the elastic–plastic analysis method and the axial and lateral deformation of the composite specimens obtained from the experimental tests, the following results can be evaluated.

4.1 Stress-strain relationships of composite column

Axial and lateral stress–strain curves for the STCC and CFST specimens with active and passive confinement are illustrated in Figs. 4 and 5, which extended to strain of 0.05 and failure point, respectively. The axial and lateral strains of the composite column are defined as the ratio of axial shortening to initial length, and the ratio of lateral deformation to initial diameter, respectively. In all the specimens, the hoop strain of the steel tube is considered as the lateral strain of the specimen. Note that in STCC specimens, the lateral strains of the concrete core and steel tube are equal due to the bonding present between the concrete and steel tube. In CFST specimens, although there may be a slight difference between the lateral strain of the steel tube and that of the concrete core at the initial steps of loading owing to their different Poisson's ratios, this disparity is reduced after the concrete cracking. The axial stress is also determined by the ratio of axial force to the cross-sectional area of the concrete core. Although in CFST

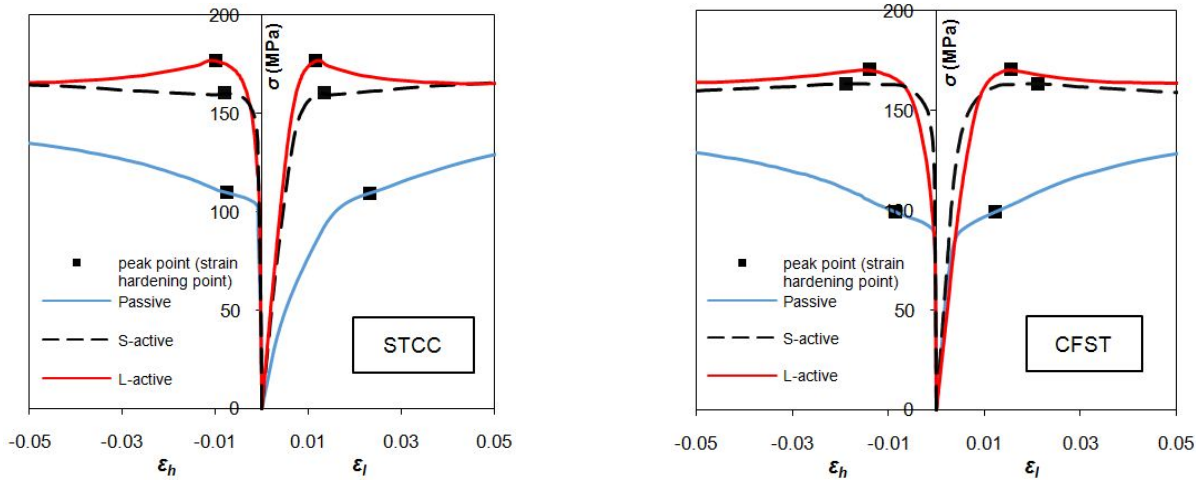

Fig. 4 Axial and lateral stress-strain curves of STCC and CFST specimens up to strain of 0.05

sections, the whole cross-section of the concrete core and steel tube participates in load-carrying, for the purpose of comparing their results with those of STCC sections, the load-carrying areas of both the sections are assumed to be equal.

With respect to the stress–strain curves of the STCC specimens in Figs. 4 and 5, the curves of the active specimens (S-active and L-active) are located considerably higher than that of the passive specimens. The compressive strength and stiffness of the active specimens are 1.6 and 2.3 times, respectively, as high as those of the passive specimens. Although the initial parts of the stress–strain curves of the passive and active CFST specimens almost coincides with each other, which leads to the same stiffness values for the both, the compressive strength of the active specimens is about 1.7 times as high as that of the passive specimens. The results indicate that prestressing by the present technique is capable of considerably improving the compressive behavior of CFST and STCC columns. It is seen in Figs. 4 and 5 that the stress–strain curves of the specimens with S-active and L-active confinement are not different, suggesting that higher prestressing levels affect the compressive behavior of the active specimens insignificantly.

The point worth noting about the STCC and CFST specimens is that the stress–strain curve of the active specimens has a clear relative peak point while there is no such a point recognizable in the passive ones. This is mainly due to the high compressive strength of concrete in the active specimens. In fact, as the compressive strength of concrete increases or the confining pressure of the steel tube decreases, the compressive behavior of the composite section approaches that of the concrete; the stress–strain curve of which has a relative peak point. In these specimens, the steel strain hardening usually occurs after the relative peak stress of the composite section has been reached. In this study, the relative peak stress of the active specimens was considered as their compressive strength, while in the passive specimens, the stress corresponding to the steel strain hardening point was taken as the compressive strength.

It can be found from Fig. 4 that the linear part of stress–strain curve for the active STCC specimens (S-active and L-active) is much more extended than that of the passive ones, which is mostly due to the high compressive strength of concrete core in the active specimens. Further-

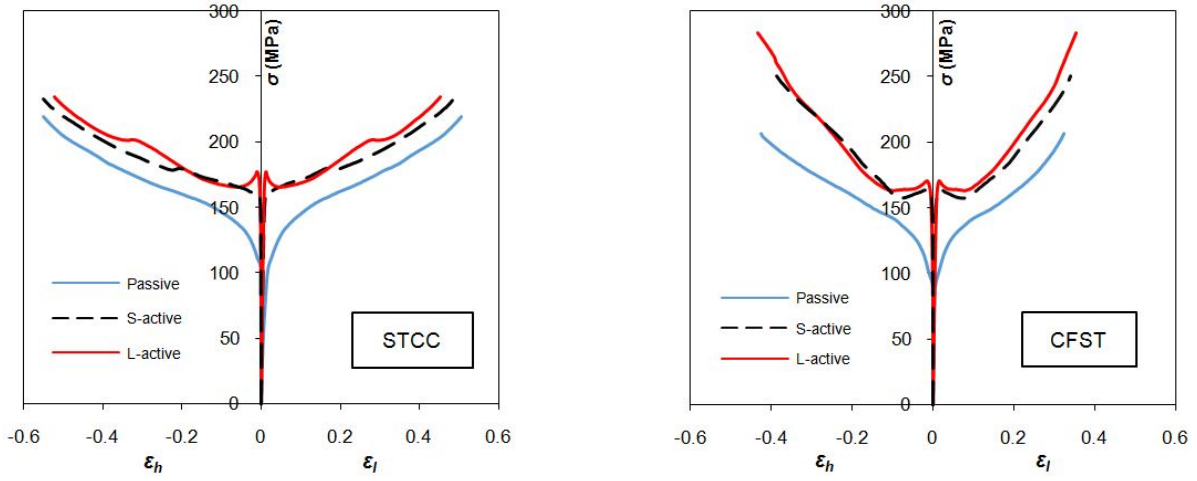

Fig. 5 Axial and lateral stress-strain curves of STCC and CFST specimens up to failure load

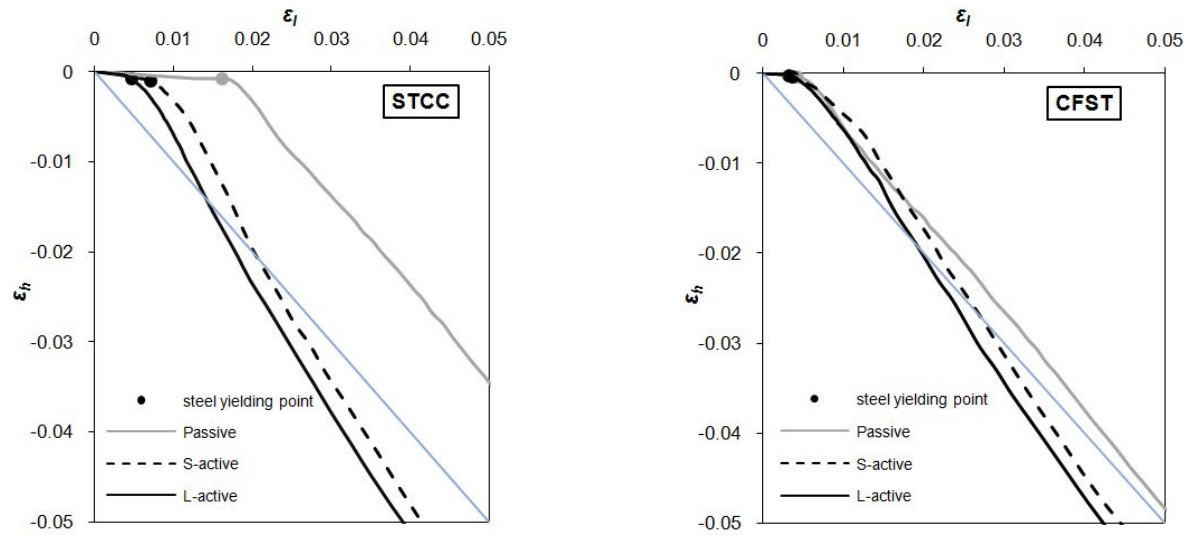

Fig. 6 Relationship between the hoop and axial strain of STCC and CFST specimens

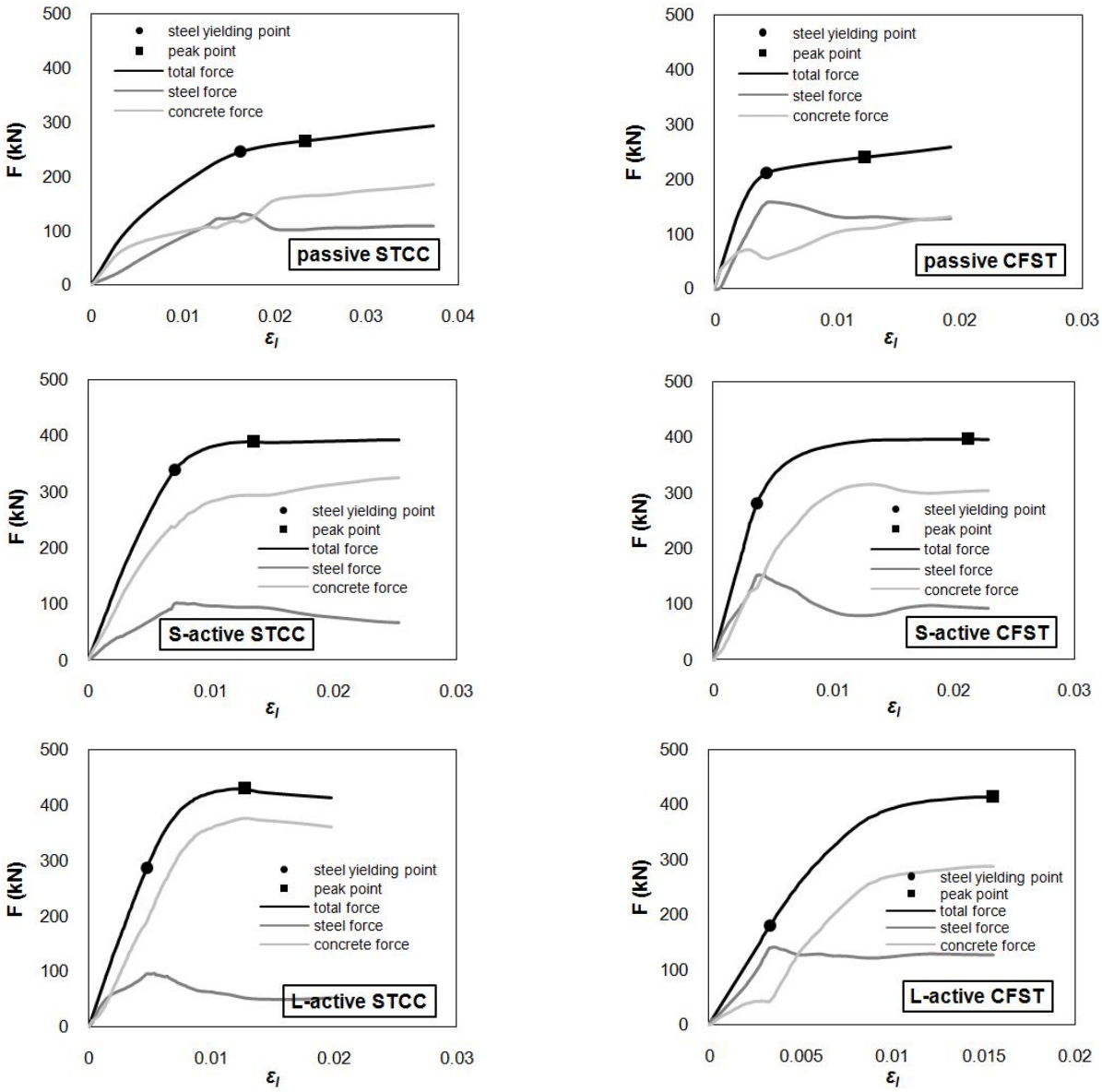

Fig. 7 Load-carrying contribution of steel tube and concrete core in STCC and CFST specimens

-more, in the CFST specimens, the stress–strain curves of both active and passive specimens have an extended linear part, mainly due to the significant role played by the steel tube in axial load-carrying from the beginning of loading.

4.2 Axial-lateral strain relationship of composite column

The relationship between the lateral strain (ε_h) and axial strain (ε_l) of the composite column for the STCC and CFST specimens is shown in Fig. 6. Regarding the figure, it is seen that the lateral strain of composite column is negligible before the steel yielding point, and increases rapidly beyond that. The increase rate in the lateral strain is almost the same in all the specimens independent of the composite section type (STCC or CFST) and the confinement type (active or passive). It can also be found that the difference between the curves is caused by the difference in the axial strain of composite columns corresponding to the steel yielding point. Moreover, according to Fig. 6, the curves of the CFST specimens with active and passive confinement are close to the bisector line of the coordinate axes. This suggests that there is a little difference between the lateral and axial strains of the CFST specimens, especially for large strain values, and hence the ratio of the lateral to axial strain (known as Poisson's ratio) is about 1. This trend is partially observed in the active STCC specimens (S-active and L-active), while in the passive ones, the lateral strains are significantly lower than their axial counterparts (Poisson's ratio is lower than 1). These results indicate that the effect of applying prestressing to the CFST columns and increasing its levels on the lateral to axial strain ratio during compressive loading can be neglected, whereas in the STCC columns, prestressing increases this ratio but changing the prestressing level does not affect it.

4.3 Load-carrying contribution of composite column components

In Fig. 7, the curves representing the relationships between the axial load-carrying portions of the composite column components, i.e., the steel tube and concrete core, as well as the total axial load applied to the composite section and the axial strain of the composite column are plotted. Considering the figure, following the steel yielding in all the specimens, the load-carrying portion of the steel tube is reduced, while that of the concrete core is increased subsequently. In the passive STCC specimens, the load-carrying portion of the concrete and steel is almost the same at the yield point, while in the passive CFST specimen, the load-carrying portion of the steel is considerably higher than that of the concrete at that point (about 3 times). However, the two load-carrying portions in the passive CFST specimen are almost equal at the end of yield stage.

In the S-active and L-active STCC specimens, the load-carrying portion of the concrete core is considerably larger than that of the steel tube during the loading, as shown in Fig. 7. This observation also holds for the S-active and L-active CFST specimens in the yielding stage. These findings indicate that prestressing the STCC and CFST columns significantly increases the load-carrying portion of the concrete core.

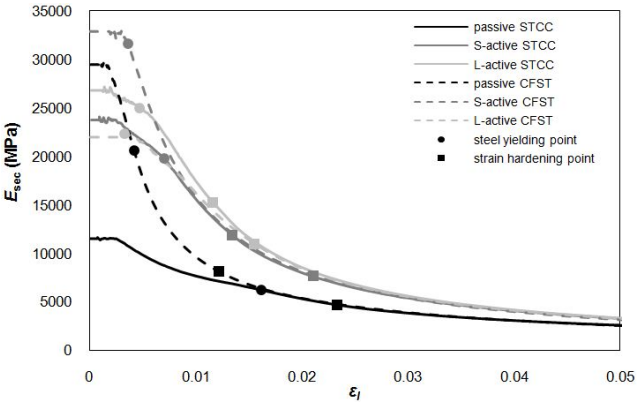

Fig. 8 Relationship between secant modulus of elasticity and axial strain of STCC and CFST specimens

4.4 Secant modulus of elasticity of composite column

The relationship between the secant modulus of elasticity (E_{sec}) and the axial strain during the loading steps for the CFST and STCC specimens with active and passive confinement is given in the form of curves in Fig. 8. Regarding the figure, the secant modulus of all the specimens exhibits a quick decrease after the steel yielding point, and after the strain hardening point, this reduction rate in the secant modulus remains almost constant in all the specimens. The horizontal line at the start of the curves specifies the linear stage of stress–strain relationship of the specimens, in which the secant modulus is almost constant.

The reduction rate in the secant modulus of the passive STCC specimen after the steel yielding point and up to the strain hardening point is lower than that of the passive CFST specimen, as can be understood in Fig. 8. This is because the steel tube stiffness having a key role in determining the stiffness of the CFST specimen is suddenly disappears in the yielding stage. However, this fact has a smaller influence on the stiffness of STCC specimens in which the main portion of stiffness belongs to the concrete core. The point worth mentioning is that the secant modulus curves of the passive STCC and CFST specimens coincide with each other after the strain hardening point, due to the conformity of the axial stress–strain curves of the passive STCC and CFST specimens after the strain hardening point, as shown in Fig. 8. In addition, the secant modulus curves of the active STCC and CFST specimens are coincident with each other in the steel yielding stage and after the strain hardening point, in particular, indicating a match between their axial stress–strain curves. These results show that the type of composite section and the prestressing level have an insignificant effect on the secant modulus of the composite specimen after the steel yielding point is reached. It can also be found from Fig. 8 that prestressing the STCC specimens increases the reduction rate of secant modulus in the yielding stage while it has no significant effect on that of the CFST specimens.

4.5 Volumetric strain of composite column

The volumetric strain of composite specimens (ε_e) can

Table 2 The results of volumetric strain

Specimen ID		Maximum volumetric strain and corresponding normalized stress		Normalized stress at $\varepsilon_e = 0$
		ε_e	σ/σ_{cc}	σ/σ_{cc}
STCC	Passive	0.0155	0.93	1.06
	S-active	0.0054	0.90	1.00
	L-active	0.0045	0.81	0.98
CFST	Passive	0.0036	0.91	0.96
	S-active	0.0049	0.86	0.96
	L-active	0.0030	0.65	0.89

be calculated using the axial and lateral strains as follows

$$\varepsilon_e = \varepsilon_l + 2\varepsilon_h \tag{20}$$

In the above equation, positive and negative values of the volumetric strain represent the contraction and expansion in the volume of specimen, respectively. The normalized axial stress (σ/σ_{cc}) vs. volumetric strain curves for the STCC and CFST specimens with active and passive confinement are illustrated in Fig. 9. Additionally, the values of the maximum volumetric strain and corresponding normalized axial stress as well as the normalized stress at the point of sign change of the volumetric strain (σ/σ_{cc} at ε_e = 0) are given in Table 2. With respect to Fig. 9, it is seen that the curve belonging to the passive CFST specimen matches that of the active CFST specimen before the maximum volumetric strain. This is due to the fact that axial and lateral stress–strain curves of the passive CFST specimen match those of the active specimens, because of the key role played by the steel tube in axial load-carrying of the CFST specimens. According to Fig. 9 and Table 2, the maximum volumetric strain values in the passive, S-active, and L-active CFST specimens are close to each other, suggesting that neither prestressing the CFST specimen nor applying high prestressing levels affects the maximum volumetric strain. Furthermore, the normalized stress for which the maximum volumetric strain occurs is the same for the passive and S-active CFST specimens, while it has a smaller relative value for the L-active specimens. The high initial hoop stress value of the steel tube in the L-active CFST specimen due to the prestressing as well as the considerable value of the longitudinal stress at the beginning of the axial loading leads to steel tube to yield, and the lateral strain to increase quickly. Hence, the volumetric strain is subsequently reduced. Based on Table 2, the normalized stress corresponding to the maximum volumetric strain in the CFST specimens with the passive, S-active, and L-active confinement type is 0.91, 0.86, and 0.65, respectively. Given that the ratio of the yield to peak compressive strength in these specimens is 0.88, 0.81, and 0.61, respectively, it can be concluded that the maximum volumetric strain occurs shortly after the steel tube yielding. Furthermore, with respect to Table 2, the change in the volumetric strain condition from contraction to expansion (ε_e = 0) for the CFST specimens occurs shortly before the peak compressive strength is reached.

With respect to the STCC curves shown in Fig. 9, it is found that the volumetric strain of the passive specimen before reaching the maximum volumetric strain is considerably higher than that of the active specimens. In Table 2, the ratio of the maximum volumetric strain in the passive STCC specimens to that of the active ones is about 3. The higher axial stiffness of concrete core in the active STCC specimens in comparison with the passive ones as well as the presence of an initial confining pressure in them leads to lower strains, and thus lower volumetric strain. This result shows that prestressing the STCC specimens by the present method significantly reduces the volumetric strain during the loading. Moreover, increasing the prestressing level has no significant effect on the volumetric strain of the STCC specimens, as shown in Fig. 9. Similar to the CFST specimens, the normalized stresses corresponding to the maximum volumetric strain in the STCC specimens having passive and S-active confinements are almost the same for the two confinement types. They are also significantly higher than that of the L-active STCC specimens. The values of normalized stress corresponding to the maximum volumetric strain in the STCC specimens with passive, S-active, and L-active confinements are 0.93, 0.90, and 0.81, respectively. Considering these results

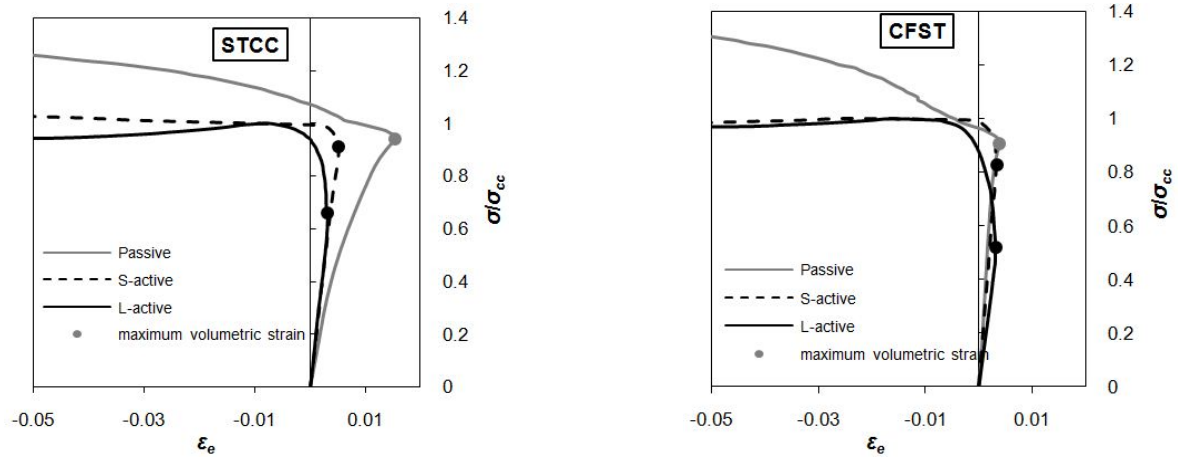

Fig. 9 Normalized stress-volumetric strain curves of STCC and CFST specimens

Fig. 10 Failure mode of STCC and CFST specimens

together with the yield to peak compressive strength ratio of the STCC specimens, it may be concluded that the maximum volumetric strain occurs shortly after the steel yielding point, similar to the CFST specimens. In addition, the inflection point of the volumetric strain from contraction to expansion for the STCC specimens occurs at the initial peak strength, as shown in Table 2.

It can be observed in Fig. 9 and Table 2 that the maximum volumetric strain of the STCC specimens is higher than that of the corresponding CFST specimens, with their ratio in the passive, S-active, and L-active specimens being 4.3, 1.1, and 1.5, respectively.

4.6 Failure mode

The Failure mode of the STCC and CFST specimens is illustrated in Fig. 10, according to which the failure modes of the specimens with passive, S-active, and L-active confinements are similar. Failure of all the STCC specimens is initiated by the steel tube rupture, and starts from the mid-height of specimens with a 45-degree angle from the horizontal axis, indicating the shear failure of steel tube. This is also the case in the thickness direction of steel tube. It can be seen in Fig. 10 that the maximum lateral deformation of the STCC specimens occurs at the mid-height, while the lateral deformation at the two ends of the specimens is insignificant due to the presence of end restraints.

Similar to the results obtained in other studies (Ellobody and Young 2006, Uy *et al*. 2011), the failure of the CFST specimens is induced by the local buckling of steel tube, as demonstrated in Fig. 10. Although the Elephant's Foot buckling mode occurs at both ends of the specimens, the maximum lateral deformation occurs at the tube mid-height.

5. Conclusions

The effect of active confinement on the compressive behaviour of STCC and CFST columns was investigated, where the axial loads are carried by concrete core and whole composite section, respectively. Three groups of STCC and CFST specimens (passive, S-active and L-active groups) with different prestressing levels were tested under axial loads. Using the elastic–plastic theory, the behaviour of the steel tube was also analyzed during elastic, yielding, and strain hardening stages. Based on the experimental results obtained in this study, the following conclusions can be drawn:

- A new method was introduced to apply confining pressure on fresh concrete by laterally prestressing steel tubes. Prestressing the STCC and CFST specimens with this method significantly improves their compressive behavior, while increasing the prestressing level has a negligible effect on the compressive behavior of the specimens.
- By applying the prestressing to the confined concrete, the linear range in the stress–strain curve of STCC specimens increased by almost twice as much, while the improvement was negligible in CFST the specimens.
- In the STCC and CFST specimens, the load carrying contribution of steel tube decreases after yielding, which increases the contribution of the concrete core accordingly. Moreover, prestressing the specimens leads to a reduced longitudinal stress, and consequently an increased load-carrying contribution of concrete, particularly after yielding of steel.
- The lateral strain at the mid-height of the STCC and CFST stub columns is insignificant up to the steel tube yielding point, after which it undergoes a rapid increase. The increase rate was equal in all specimens and was not affected by the type of composite section (STCC or CFST) and confinement type (active or passive).
- Applying prestressing to the CFST specimens has a negligible effect on the lateral to axial strain ratio of the composite column during compressive loading; however, it significantly increases this ratio in the STCC specimens. The secant modulus of elasticity of all the composite specimens is reduced after the steel yielding point is reached. Additionally, after the steel strain hardening point, the rate of decrease in the secant modulus of elasticity remains almost constant.
- While prestressing has an insignificant effect on the maximum volumetric strain of the CFST specimens, it can significantly (about 70%) reduce the maximum volumetric strain of the STCC specimens. The maximum volumetric strain of the STCC and CFST specimens occurs shortly after the steel yielding point. Also, conversion of the volumetric strain from the contraction into the expansion mode ($\varepsilon_e = 0$) occurs near the steel strain hardening point.
- The dominant failure mode in all STCC specimens was due to the rupture of steel tube. But the CFST specimens mainly failed by the local buckling of the steel tube in the elephant's foot mode at two ends of the specimens.

References

Abed, F., Alhamaydeh, M. and Abdalla, S. (2013), "Experimental and numerical investigations of the compressive behavior of concrete filled steel tubes (CFSTs)", *J. Constr. Steel Res*., **80**, 429-439.

Aboutaha, R.S. and Machado, R. (1998), "Seismic resistance of

steel confined reinforced concrete (SCRC) columns", *The Structu*. *Des*. *Tall Build*., **7**(3), 251-260.
ACI Committee 211.1-91 (2000), Standard practice for selecting proportions for normal, heavyweight, and mass concrete; *ACI manual of concrete practice*, *Part 1*. *Michigan* (*USA*)*: American Concrete Institute*, 38 p.
ASTM C39/C39M (2002), Standard test method for compressive strength of cylindrical concrete specimens; *Annual Book of ASTM Standard 04*.
Chang, X., Huang, C.K. and Chen, Y.J. (2009), "Mechanical performance of eccentrically loaded prestressing concrete filled circular steel tube columns by means of expansive cement", *Eng*. *Struct*., **31**(11), 2588-2597.
Ellobody, E. and Young, B. (2006), "Design and behaviour of concrete-filled cold-formed stainless steel tube columns", *J*. *Eng*. *Struct*., **28**(5), 716-728.
Fu, Z., Ji, B., Lv, L. and Yang, M. (2011), "The Mechanical Properties of Lightweight Aggregate Concrete Confined by Steel Tube", *Geotechnical Special Publication No*. *219*, *ASCE*, 33-39.
Han, L.H., Yao, G.H., Chen, Z.P. and Yu, Q. (2005), "Experimental behaviour of steel tube confined concrete (STCC) columns", *Steel Compos*. *Struct*., *Int*. *J*., **5**(6), 459-484.
Hosford, W. (2010), *Solid Mechanics*, University of Michigan, Emeritus, Cambridge University Press, 262 p.
Hua, W., Wang, H.J. and Hasegawa, A. (2014), "Experimental study on reinforced concrete filled circular steel tubular columns", *Steel Compos*. *Struct*., *Int*. *J*., **17**(4), 517-533.
Huang, Y., Xiao, J. and Zhang, C. (2012), "Theoretical study on mechanical behavior of steel confined recycled aggregate concrete", *J*. *Constr*. *Steel Res*., **76**, 100-111.
Janke, L., Czaderski, C., Ruth, J. and Motavalli, M. (2009), "Experiments on the residual load-bearing capacity of prestressed confined concrete columns", *Eng*. *Struct*., **31**(10), 2247-2256.
Kim, J.K., Kwak, H.G. and Kwak, J.H. (2013), "Behavior of hybrid double skin concrete filled circular steel tube columns", *Steel Compos*. *Struct*., *Int*. *J*., **14**(2), 191-204.
Krstulovic-Opara, N. and Thiedeman, P.D. (2000), "Active confinement of concrete members with self-stressing composites", *ACI Mater*. *J*., **97**(3), 297-308.
Lai, M.H. and Ho, J.C.M. (2014), "Confinement effect of ring-confined concrete-filled-steel-tube columns under uni-axial load", *J*. *Eng*. *Struct*., **67**, 123-141.
Moghaddam, H., Samadi, M., Pilakoutas, K. and Mohebbi, S. (2010), "Axial compressive behavior of concrete actively confined by metal strips; Part A: Experimental study", *Mater*. *Struct*., **43**(10), 1369-1381.
Mokari, J. and Moghadam, A.S. (2008), "Experimental and theoretical study of reinforced concrete columns with poor confinement retrofitted by thermal post tension steel jacketing", *J*. *Appl*. *Sci*., **8**(24), 4579-4586.
Mortazavi, A.A., Pilakoutas, K. and Son, K.S. (2003), "RC column strengthening by lateral pre-tensioning of FRP", *Constr*. *Build*. *Mater*., **17**(6), 491-497.
Nematzadeh, M. and Naghipour, M. (2012), "Compressive strength and modulus of elasticity of freshly compressed concrete", *Constr*. *Build*. *Mater*., **34**, 476-485.
Nematzadeh, M., Fazli, S., Naghipour, M. and Jalali, J. (2017), "Experimental study on modulus of elasticity of steel tube-confined concrete stub columns with active and passive confinement", *Eng*. *Struct*., **130**, 142-153.
Shinohara, Y. (2008), "Effect of transverse prestressing on shear behaviors of high-strength concrete columns", *Proceedings of the 14th World Conference on Earthquake Engineering*, Bejing, China, October.
Shin, M. and Andrawes, B. (2010), "Experimental investigation of actively confined concrete using shape memory alloys", *Eng*. *Struct*., **32**(3), 656-664.
Tokgoz, S. and Dundar, C. (2010), "Experimental study on steel tubular columns in-filled with plain and steel fiber reinforced concrete", *Thin-Wall*. *Struct*., **48**(6), 414-422.
Uy, B., Tao, Z. and Han, L.H. (2011), "Behaviour of short and slender concrete-filled stainless steel tubular columns", *J*. *Constr*. *Steel Res*., **67**(3), 360-378.
Yu, Q., Tao, Z., Liu, W. and Chen, Z.-B. (2010), "Analysis and calculation of steel tube confined concrete (STCC) stub columns", *J*. *Constr*. *Steel Res*., **66**(1), 53-64.
Wan, C.Y. and Zha, X.X. (2016), "Nonlinear analysis and design of concrete-filled dual steel tubular columns under axial loading", *Steel Compos*. *Struct*., *Int*. *J*., **20**(3), 571-597.

CC